Journal of Alloys and Compounds 509 (2011) 3262–3268

Contents lists available at ScienceDirect

Journal of Alloys and Compounds

journal homepage: www.elsevier.com/locate/jallcom

Effect of Si, Pd and La additions on glass forming ability and thermal stability of Zr–Ni-based amorphous alloys

Yan Wang*, Jingfu Wang, Cancan Li

School of Materials Science and Engineering, University of Jinan, 106 Jiwei Road, Jinan 250022, PR China

ARTICLE INFO

Article history:
Received 13 August 2010
Received in revised form 7 December 2010
Accepted 7 December 2010
Available online 14 December 2010

Keywords:
Amorphous alloys
Minor addition
Melt spinning
Glass forming ability
Thermal stability

ABSTRACT

In the present paper, the influence of minor additions of Si, Pd and La with representative atomic sizes on glass forming ability (GFA) and thermal stability of Zr–Ni-based amorphous alloys has been investigated using X-ray diffraction (XRD), differential scanning calorimetry (DSC), transmission electron microscopy (TEM) and high resolution TEM (HRTEM). The results show that minor additions of La, Pd and Si can improve GFA of Zr–Ni-based alloys and La exhibits the optimum effect on enhancing GFA. The efficient cluster packing model can well explain the correlation between atomic sizes of additional elements and GFA of amorphous alloys. In addition, the relationship of the atomic size between the additional element and Zr has a more important effect on GFA than that between the additional element and Ni. The activation energy for crystallization of the Zr–Ni-based amorphous alloys with Si, Pd and La additions is obviously higher than that of the $Zr_{66.7}Ni_{33.3}$ amorphous alloy, and increases with decreasing distance between neighboring atoms. The thermal stability has a relation with topological short-range ordering of amorphous alloys. The proper addition of small atoms is preferential to enhance thermal stability of amorphous alloys due to stronger short-range ordering. Moreover, the small or intermediate atom addition can produce even better effect on thermal stability than the large atom addition.

© 2010 Elsevier B.V. All rights reserved.

1. Introduction

To this day, many researchers have great interest in the origin of glass forming ability (GFA) of amorphous alloys. Minor alloying additions or microalloying technologies are key metallurgical practices and dominant concepts for developing new metallic crystalline materials in the late half of the 20th century. It has been recently reported that appropriate minor alloying additions are very effective in increasing GFA, and enhancing thermal stability and mechanical properties of some metallic glasses [1–6]. Moreover, the minor addition approach can also represent a feasible way to develop and design novel amorphous alloys. Although Wang and co-workers [7–10] have studied the influence of additions of elements with different atomic sizes on formation and properties of bulk metallic glasses (BMGs), the origin of additional effects has not been well addressed. Our previous findings have shown that minor additions of C or Au can effectively improve GFA of Zr–Ni-based alloys by mechanical alloying (MA) [11,12]. However, the mechanism of the minor addition lacks a fundamental theory in glass formation and properties tailoring. It has been suggested that the additional atomic number, size mismatch or chemical affinity with constitutional elements may affect the metallic glass formation and its properties. To further study the correlation between atomic size and GFA or thermal stability of Zr–Ni amorphous alloys prepared by melt-spinning, the additional elements Si, Pd and La with different atomic sizes have been designedly selected to substitute for Zr. According to atomic radii, these elements can be classified into three groups [13]: large atoms (La, 0.18790 nm; Zr, 0.16025 nm [14]), intermediate atoms (Pd, 0.13754 nm; Ni, 0.12459 nm [14]) and small atoms (Si, 0.11530 nm [14]). The additions of a suitable amount of Si, Ni and La would lead to a sequential order in the atomic size (La > Zr > Pd > Ni > Si). In the present work, we report the effect and mechanism of microalloying on GFA and thermal stability of Zr–Ni-based amorphous alloys. In addition, the correlation between atomic sizes of additional elements and related effects has also been discussed in order to further improve GFA and thermal stability of Zr–Ni amorphous alloys.

2. Experimental

Ingots of $Zr_{66.7-x}Ni_{33.3}M_x$ (M = Si, Pd and La and x = 0, 1, 3 at.%) alloys were obtained by melting nominal amounts of pure Zr (99.9 wt.%), Ni (99.9 wt.%), Si (99.99 wt.%), Pd (99.9 wt.%) and La (99.9 wt.%) in a vacuum arc furnace. Using a single roller melt spinning apparatus, the pre-alloyed ingots were remelted in a quartz tube by high-frequency induction heating and then melt-spun onto a copper roller with a diameter of 0.22 m at rotation speeds of 1000, 2000 and 3000 revolutions per minute (rpm). The temperature of the ejected melt was controlled as the same for any $Zr_{66.7-x}Ni_{33.3}M_x$ alloy at different applied rotation speeds. Here, different rotation speeds were utilized to obtain different cooling rates during rapid solidi-

* Corresponding author. Tel.: +86 531 82765473; fax: +86 531 87974453.
E-mail address: mse_wangy@ujn.edu.cn (Y. Wang).

0925-8388/$ – see front matter © 2010 Elsevier B.V. All rights reserved.
doi:10.1016/j.jallcom.2010.12.035

fication, and further to examine GFA of Zr–Ni alloys with elemental additions. The phase constitution of the as-quenched ribbons was identified by X-ray diffraction (XRD, Rigaku D/max-RB) using Cu Kα radiation (λ = 0.15406 nm). The peak position for the first maximum on the XRD pattern was determined by fitting the peak to a Gaussian profile using one Origin software. The thermal stability was investigated by a differential scanning calorimetry (DSC, Netzsch 404) at various heating rates of 5, 10, 15, 20 and 30 K min^{-1} under a continuous flow of purified argon. The microstructure of the ribbons was characterized using transmission electron microscopy (TEM, Philips CM20) and high resolution TEM (HRTEM, FEI Tecnai G2). The foils for TEM and HRTEM observations were punched directly from the melt-spun ribbons and prepared by ion milling.

3. Results and discussion

Fig. 1 shows XRD patterns of the melt-spun $Zr_{66.7-x}Ni_{33.3}M_x$ (M = Si, Pd and La and x = 0, 1, 3 at.%) alloy ribbons quenched at different rotation speeds. The melt-spun $Zr_{66.7}Ni_{33.3}$ alloy containing no additional element is composed of a mixture of amorphous and crystalline phases at 1000 rpm, the latter being bcc-Zr_2Ni (Fig. 1A(a)). The as-quenched structure of the Zr–Ni alloy with 1 at.% Si or Pd addition is similar to that of the $Zr_{66.7}Ni_{33.3}$ alloy at this low rotation speed, which is not a fully amorphous phase (Fig. 1A (b and d)). With the 3 at.% Si or Pd addition, however, the melt-spun alloys quenched at 1000 rpm comprise a fully amorphous phase (Fig. 1A (c and e)). In addition, a fully amorphous phase can be identified in the melt-spun Zr–Ni alloys with 1 and 3 at.% La additions quenched at 1000 rpm (Fig. 1A (f and g)). It is obvious that minor additions of La, Pd and Si can improve the GFA of the $Zr_{66.7}Ni_{33.3}$ alloy. For La, 1 at.% addition is enough for formation of a fully amorphous phase in the melt-spun Zr–Ni alloys. For Pd and Si, 3 at.% addition is necessary to obtain a fully amorphous phase in the as-quenched alloys. With increasing rotation speed to 2000 and 3000 rpm, the XRD patterns of the melt-spun Zr–Ni-based alloy ribbons are shown in Fig. 1(B and C). All the patterns show diffuse broad peaks, indicating that all the melt-spun alloys are fully amorphous. However, their diffraction angles (2θ) for the first maximum on the XRD patterns have different shifts, and this will be discussed in the following.

To verify the XRD results, some samples were selected to be examined using TEM and selected-area electron diffraction (SAED). Fig. 2 shows TEM bright-field images and corresponding SAED patterns of the melt-spun $Zr_{66.7}Ni_{33.3}$ and $Zr_{65.7}Ni_{33.3}La_1$ alloy ribbons obtained at the rotation speed of 1000 rpm. Fig. 2a shows some fine randomly dispersed nanocrystals in an amorphous matrix from the melt-spun $Zr_{66.7}Ni_{33.3}$ alloy. The SAED pattern consists of several bright diffraction spots superimposed on a diffuse halo, indicating a mixture of crystalline and amorphous phases, as shown in Fig. 2b. Fig. 2c shows a typical microstructure of the melt-spun $Zr_{65.7}Ni_{33.3}La_1$ alloy obtained at the rotation speed of 1000 rpm, and the corresponding SAED pattern is a diffuse halo indicating the amorphous characteristic of the alloy (Fig. 2d). HRTEM observations further verify the above results. Fig. 3a shows a nanocrystal with a size of around 30 nm embedded in the amorphous matrix of the melt-spun $Zr_{66.7}Ni_{33.3}$ alloy. The corresponding fast Fourier transformation (FFT) pattern consists of sharp diffraction spots together with a diffuse halo, consistent with the microstructure (inset of Fig. 3a). Fig. 3b shows an isotropic maze pattern of the melt-spun $Zr_{65.7}Ni_{33.3}La_1$ alloy, which is typical of an amorphous structure. The corresponding FFT pattern exhibits a diffuse halo (inset of Fig. 3b).

Generally, large negative heat of mixing (ΔH_{mix}) among constituent elements is a factor that may benefit GFA. Large negative values of ΔH_{mix} can enhance interactions among components and promote chemical short-range ordering, which can improve local packing efficiency and restrain long range diffusion of atoms. The values of ΔH_{mix} between Zr and other elements in the Zr–Ni–Si, Zr–Ni–Pd and Zr–Ni–La systems are available in Ref. [15] and listed

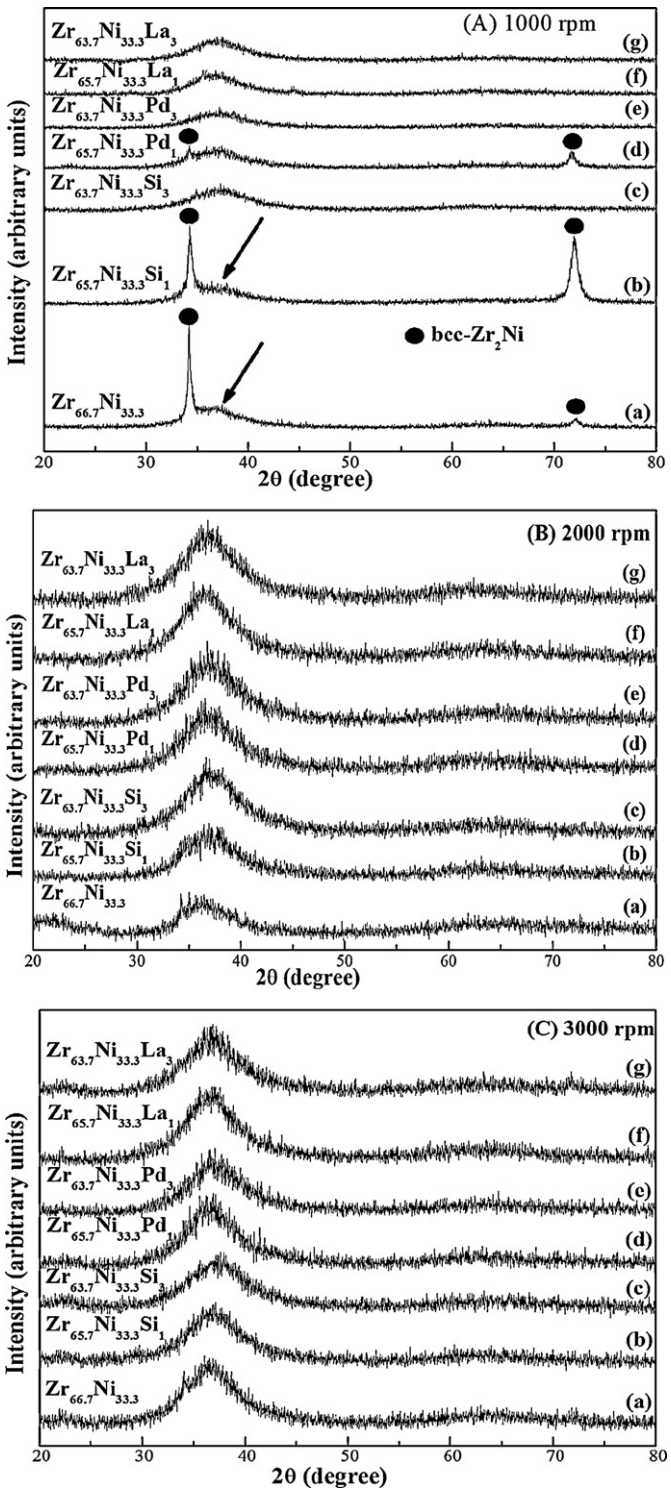

Fig. 1. XRD patterns of the melt-spun $Zr_{66.7-x}Ni_{33.3}M_x$ (M = Si, Pd and La and x = 0, 1, 3 at.%) ribbons obtained at different rotation speeds. (A) 1000 rpm, (B) 2000 rpm and (C) 3000 rpm.

in Table 1. In spite of the positive ΔH_{mix} (13 kJ mol^{-1}) between Zr and La [15], the La addition (1 or 3 at.%) can improve GFA of Zr–Ni–La alloys. In comparison to Zr–Ni–La, the Zr–Ni–Si and Zr–Ni–Pd systems have more negative ΔH_{mix} (Zr–Si: −84 kJ mol^{-1} and Zr–Pd: −91 kJ mol^{-1}) [15] and should have higher GFA. In fact, however, the GFA of the Zr–Ni–Si and Zr–Ni–Pd systems is not better than Zr–Ni–La. Therefore, the negative ΔH_{mix} criterion is not effective to explain the effect of elemental additions on GFA

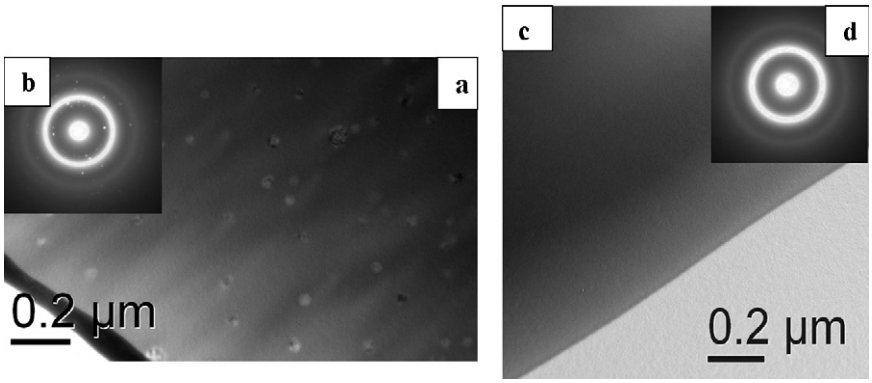

Fig. 2. TEM bright-field images showing the microstructure of the melt-spun (a) $Zr_{66.7}Ni_{33.3}$ and (c) $Zr_{65.7}Ni_{33.3}La_1$ alloy ribbons quenched at 1000 rpm. (b and d) SAED patterns corresponding to (a and c), respectively.

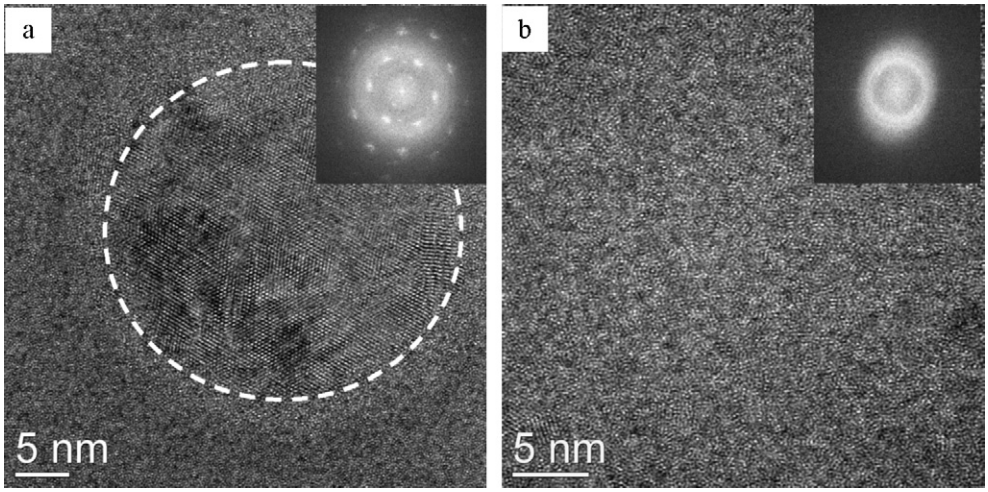

Fig. 3. HRTEM images showing the microstructure of the melt-spun (a) $Zr_{66.7}Ni_{33.3}$ and (b) $Zr_{65.7}Ni_{33.3}La_1$ alloy ribbons quenched at 1000 rpm. Insets: corresponding FFT patterns.

Table 1
The values of heat of mixing (ΔH_{mix}) between two constituents for the Zr–Ni–Si, Zr–Ni–Pd and Zr–Ni–La alloy systems [15].

Alloy systems (A–B–C)	ΔH_{mix} (kJ mol^{-1})		
	A–B	A–C	B–C
Zr–Ni–Si	−49	−84	−40
Zr–Ni–Pd	−49	−91	0
Zr–Ni–La	−49	13	−27

of Zr–Ni-based amorphous alloys. As it has already been demonstrated by several authors, the negative ΔH_{mix} cannot explain the additional effect on improving GFA of some amorphous alloys [16,17]. Moreover, it has been argued that the addition of elements with positive heat of mixing can also increase GFA [18]. It should be noted that a miscibility gap may occur in a ternary alloy system where the ΔH_{mix} for any couple of constituent elements is negative. Abe et al. [19] have pointed out that if the ΔH_{mix} for the various couples of elements in a ternary system is significantly more negative than the others, a miscibility gap may occur in the liquid phase and will reduce the GFA of the ternary system. The ΔH_{mix} of Zr–Si is much more negative than that of either Zr–Ni or Ni–Si in the Zr–Ni–Si system, and a similar scenario can also be found in the Zr–Ni–Pd system (Table 1). According to the argument of Abe et al. [19], it is reasonable to assume that a miscibility gap may appear in the liquid phase of Zr–Ni–Si and Zr–Ni–Pd, which thus decreases their GFA.

Recently, a structural model has been proposed by Miracle [20] for metallic glasses based on efficient filling of space by solute-centered clusters. The model shows that solutes possess specific sizes relative to solvent atoms to produce efficient atomic packing. Efficient packing is enabled for N solvent atoms when the solute-to-solvent radius ratio R attains to specific and predictable values R_N^*. Clusters with $N = 11$ and $N = 12$ (such as icosahedron or defective icosahedron) have solutes that are nearly topologically identical, and so it is proposed that clusters with $N = 11$ will not be observed in favor of more efficiently packed icosahedra. Further, clusters with $N = 13$ and $N = 14$ are not common. Table 2 lists the atomic size ratio R, the closest value R_N^* for the ratio R, coordination number N and the specific value between $(R_N^* - R)$ and

Table 2
Calculated radius ratio $R = (r_{solute}/r_{solvent})$, the closest R_N^* for the ratio R, corresponding coordination number N and the specific value between $(R_N^* - R)$ and R for the Zr–Ni–Si, Zr–Ni–Pd and Zr–Ni–La alloy systems.

Solvent–solute	R	R_N^* [20]	N [20]	$\left\|R_N^* - R/R\right\| \times 100\%$
Zr–Ni	0.810	0.799	10[a]	1.36
Zr–Si	0.646	0.617	8[a]	4.49
Ni–Si	0.800	0.799	10[a]	0.13
Zr–Pd	0.892	0.884	11	0.90
Ni–Pd	1.102	1.116	15[a]	1.27
Zr–La	1.184	1.183	16[a]	0.08
Ni–La	1.461	1.433	20[a]	1.92

[a] Clusters typically expected in metallic glasses.

R for two arbitrary alloying elements. It is necessary to point out that the atomic sizes of studied elements during this discussion are referred according to the literature [20]. Based upon calculated data and experimental results, Miracle's model can well explain GFA of Zr–Ni–Si, Zr–Ni–Pd and Zr–Ni–La alloys. The least specific value (0.08) between ($R_N^* - R$) and R is obtained for the Zr–La system. The R value of Zr–La (1.184) highly approaches to the predictable value R_N^* (1.183), so the Zr–Ni–La alloy system possesses more efficient atomic packing than other alloy systems in this paper. These calculated data are in agreement with our experimental results that the Zr–Ni–La alloy has the highest GFA when using the melt-spinning method. Although both Zr–Ni–Pd and Zr–Ni–Si have low specific values (0.90 and 0.13, respectively), the clusters with $N = 11$ for the former will not be observed in favor of more efficiently packed icosahedra and the low specific value of the latter is shown by Ni–Si (not Zr–Si). Therefore, it can be suggested that the relation between the matrix (Zr) and additional element has a more important effect on GFA of $Zr_{66.7-x}Ni_{33.3}M_x$ alloys than that between Ni and the additional element. Thus the Zr–Ni–Pd and Zr–Ni–Si systems have lower GFA than Zr–Ni–La (Fig. 1A).

Fig. 4 shows DSC curves of $Zr_{66.7-x}Ni_{33.3}M_x$ (M = Si, Pd and La and $x = 0$, 1, 3 at.%) amorphous alloys quenched at 3000 rpm at different heating rates of 5, 10, 15, 20, and 30 K min^{-1}. Exothermic peaks can be observed on each DSC trace corresponding to crystallization of the amorphous phase in these melt-spun alloys. Moreover, one, two and even three exothermic peaks can be seen on the DSC traces, indicating one-step or multi-step (two-step, three-step) crystallization behaviors of the present $Zr_{66.7-x}Ni_{33.3}M_x$ amorphous alloys. The crystallization process is one-step for the $Zr_{66.7}Ni_{33.3}$ amorphous alloy without any addition (Fig. 4a). In comparison, a three-step crystallization behavior can be discerned for the $Zr_{65.7}Ni_{33.3}Pd_1$ amorphous alloy despite the overlapping of three exothermic peaks (Fig. 4d). It is obvious that the elemental addition of Si, Pd and La has a significant influence on the crystallization behavior of the present $Zr_{66.7-x}Ni_{33.3}M_x$ amorphous alloys. In addition, it should be noted that the exothermic peaks on the DSC traces of the $Zr_{65.7}Ni_{33.3}La_1$ amorphous alloy show an abnormal profiles (Fig. 4f), which may be associated with its unique crystallization behavior. The underlying reason needs to be further clarified in the later work. From Fig. 4, it can be seen that the onset crystallization temperature (T_x) and the crystallization peak temperature (T_p) of the maximum exothermic peak increase as the heating rate increases (as marked by arrows in Fig. 4).

The effective activation energy for crystallization of the $Zr_{66.7-x}Ni_{33.3}M_x$ amorphous alloys can be evaluated by the Kissinger equation [21]:

$$\ln\left(\frac{T^2}{\beta}\right) = \frac{E_a}{RT} + C \quad (1)$$

where T is the specific temperature, β is the heating rate, R is the gas constant, and E_a is the activation energy. It is known that the onset crystallization temperature is associated with the nucleation process, and the peak temperature is related to the growth process. It may presume that the activation energies deduced from the onset crystallization and peak temperatures respectively, represent the activation energy for nucleation and growth [22]. The T_x value of the main exothermic peak on the DSC traces cannot be obtained accurately, but the T_p value corresponding to the main exothermic peak can be well determined from the DSC traces and was used to evaluate the activation energy for crystallization of the present $Zr_{66.7-x}Ni_{33.3}M_x$ (M = Si, Pd and La and $x = 0$, 1, 3 at.%) amorphous alloys quenched at 3000 rpm. By substituting T_p for T in the Eq. (1), the activation energy for crystallization can be determined from the slope of a plot of the $\ln(T_p^2/\beta)$ against $1/T_p$. The $\ln(T_p^2/\beta)$ as a function of $1/T_p$ is plotted in Fig. 5. On the whole, a good linear relationship can be obtained for all the Kissinger plots of the $Zr_{66.7-x}Ni_{33.3}M_x$ (M = Si, Pd and La and $x = 0$, 1, 3 at.%) amorphous alloys, especially for the $Zr_{66.7}Ni_{33.3}$, $Zr_{65.7}Ni_{33.3}Si_1$, $Zr_{65.7}Ni_{33.3}Pd_1$ and $Zr_{63.7}Ni_{33.3}La_3$ amorphous alloys (Fig. 5). And for the $Zr_{63.7}Ni_{33.3}Si_3$, $Zr_{63.7}Ni_{33.3}Pd_3$ and $Zr_{65.7}Ni_{33.3}La_1$ amorphous alloys, some data points deviate from the linear relationship, but well distribute at both sides of the linear plot (Fig. 5c, e and f). The calculated E_a values are shown in Fig. 6. It can be seen that the E_a value for the Si, Pd and La additions is obviously higher than that of $Zr_{66.7}Ni_{33.3}$, except the 1 at.% La addition. This indicates that the addition of Si, Pd and La can enhance the thermal stability of Zr–Ni–based amorphous alloys. It is worth noting that partial substitution of La for Zr exhibits the optimum effect on improving GFA, but the as-obtained amorphous alloy does not possess the highest thermal stability. On the other hand, $Zr_{63.7}Ni_{33.3}Si_3$ has the highest E_a value (441 ± 48 kJ mol^{-1}), implying that the 3 at.% Si addition has the best effect on the thermal stability of the amorphous alloy against crystallization. In addition, the effect of the Pd addition on the thermal stability is also superior to the La addition. So it can be noted that the small or intermediate atom additions produce even better effects on thermal stability than the large atom additions. This demonstrates that GFA has no positive correlation with thermal stability for the present $Zr_{66.7-x}Ni_{33.3}M_x$ (M = Si, Pd and La and $x = 0$, 1, 3 at.%) amorphous alloys. Madge and Greer [23] have discussed the reasons for Mg-based glasses based upon the appearance of quenched-in nuclei.

It is known that the diffraction angle for the first maximum on an XRD pattern is related to the nearest interatomic distance, following the relation $1.23\lambda = 2d_m \sin\theta$ (where λ is the wavelength of X-ray and equals to 0.15406 nm here, θ is the peak position corresponding to the first maximum on the XRD pattern, d_m is the distance between neighboring atoms, and 1.23 is a correction factor used for liquid and amorphous solids) [24]. The value of d_m obtained from the above relationship can be considered as an average TM–TM (for example, Zr–Zr, Zr–Ni and Ni–Ni in this work) nearest-neighbor distance determined by 2θ. Here, we would study the relation between variation tendency of d_m and E_a for the Zr–Ni-based amorphous alloys, and further analyze the relationship between thermal stability and topological short-range ordering of these amorphous alloys with different atomic sizes of elemental additions. Fig. 6 shows the variation of E_a values as a function of d_m for the melt-spun $Zr_{66.7-x}Ni_{33.3}M_x$ (M = Si, Pd and La and $x = 0$, 1, 3 at.%) amorphous alloys obtained at 3000 rpm. From Fig. 6, it can be seen that the distance between neighboring atoms (d_m) for the present Zr–Ni-based amorphous alloys follows an approximately contrary tendency compared to the variation of activation energy for crystallization (E_a) of these amorphous alloys with different elemental additions. Namely, the amorphous alloy has a larger E_a value and also has a smaller d_m value. However, the 1 at.% La addition leads to an exceptional variation trend, which may be correlated with the unusual profiles of the main exothermic peaks on the DSC traces of the $Zr_{65.7}Ni_{33.3}La_1$ amorphous alloy (Fig. 4f). The thermal stability (E_a) increases with decreasing average nearest-neighbor distance (d_m). Thus it can be suggested that there exists a correlation between thermal stability and topological short-range ordering of amorphous alloys. This result obtained is in good agreement with the reports by Inoue et al. [25–27] and Park et al. [28]. They have argued that the thermal stability of an amorphous phase can be enhanced with increasing topological short-range ordering.

It should be noted that the atomic radius of Si is smaller than that of both Zr and Ni, and it is predicted that Si has a higher diffusivity in Zr and Ni. So the substitution of Si for Zr in the Zr–Ni amorphous alloys can cause more obvious lattice contraction leading to more compact configuration and markedly increase thermal stability of the amorphous phase. The 1 at.% Si substitution for Zr does not

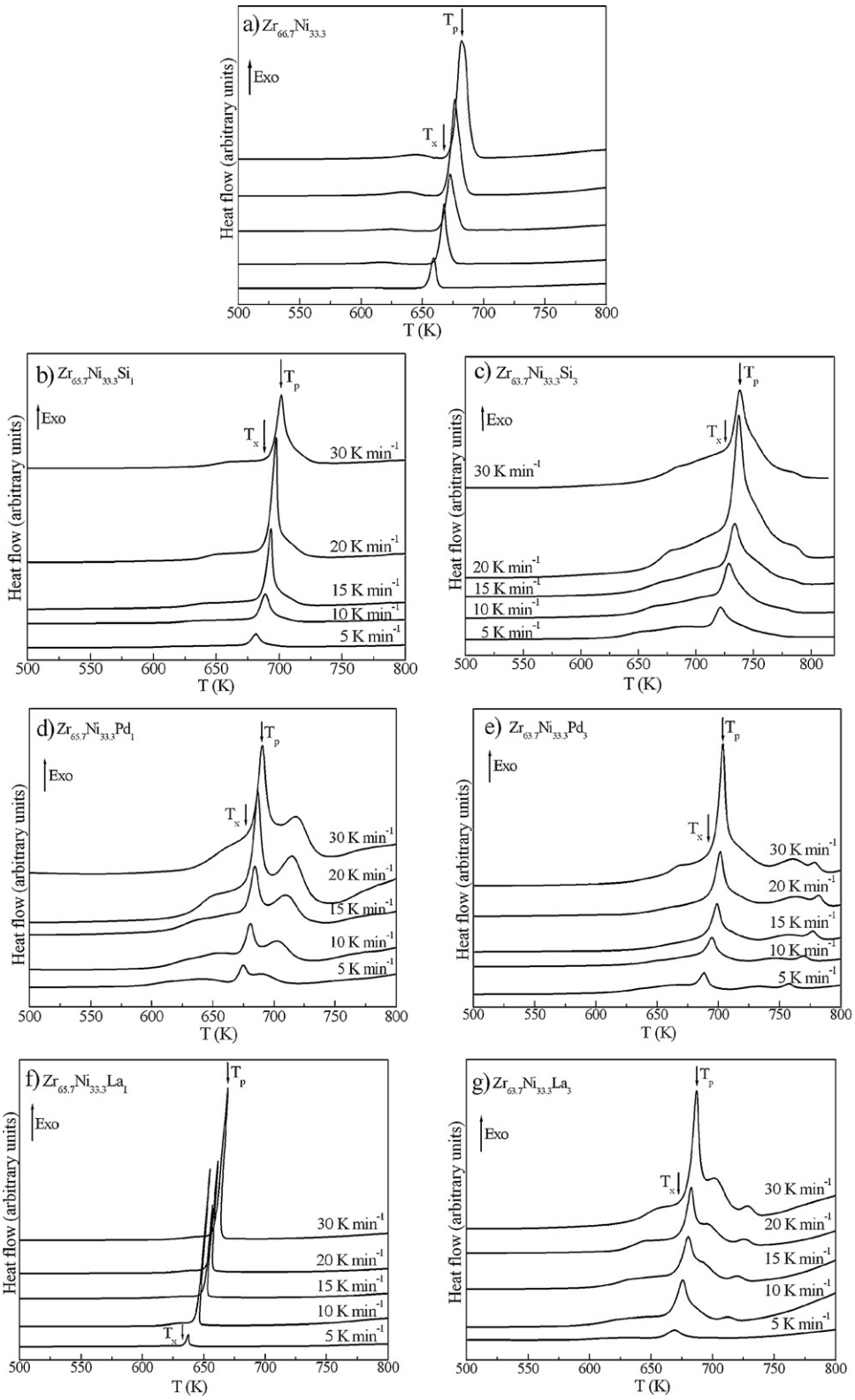

Fig. 4. DSC curves of the $Zr_{66.7-x}Ni_{33.3}M_x$ (M = Si, Pd and La and x = 0, 1, 3 at.%) amorphous alloys quenched at 3000 rpm.

remarkably enhance thermal stability, which may be explained by a weak hindering effect of a small quantity of Si atoms on the atomic mobility of diffusing species in the matrix. In comparison with the 1 at.% Si addition, the addition of 3 at.% Si may further enhance the packing density. In addition, due to their strong atomic bonding with metallic elements, proper additions of metalloid atoms (such as Si in the present work) can enhance the short-range compositional ordering (chemical short-range ordering). Therefore, the rearrangement of atoms in the Zr–Ni–Si amorphous alloys becomes much more difficult and the Si addition is beneficial to thermal stability of amorphous alloys. Pd as an intermediate atom can easier diffuse into the interstice of Zr atoms than large atom La,

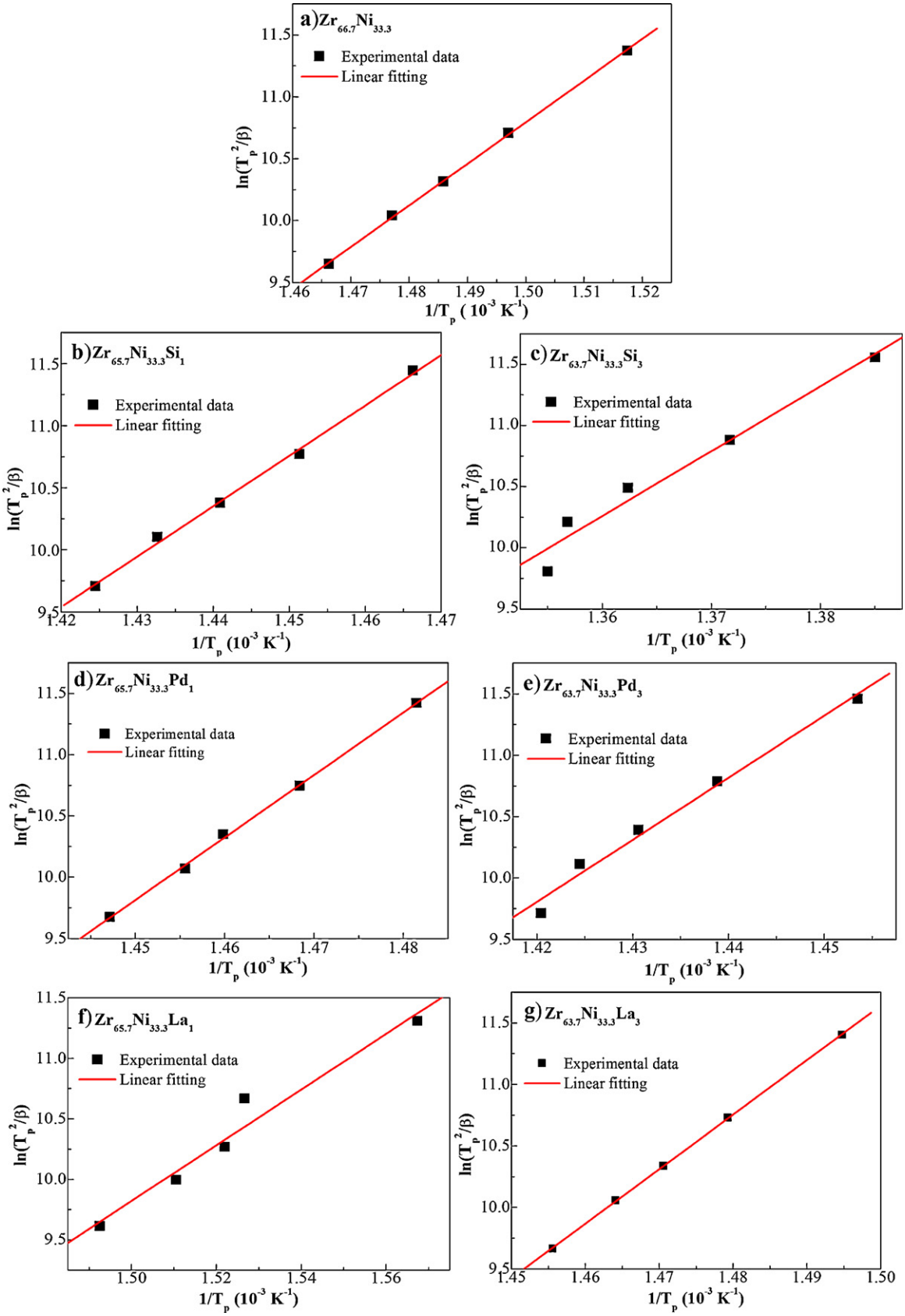

Fig. 5. Kissinger plots ($\ln(T_p^2/\beta)$ vs. $1/T_p$) for the $Zr_{66.7-x}Ni_{33.3}M_x$ (M = Si, Pd and La and x = 0, 1, 3 at.%) amorphous alloys quenched at 3000 rpm.

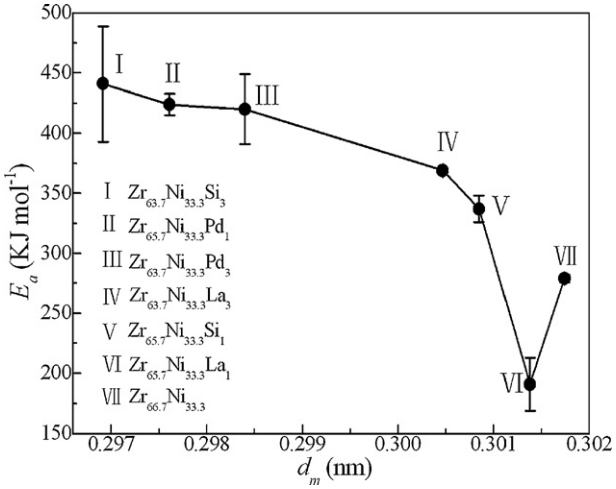

Fig. 6. Variation of E_a values as a function of d_m for the melt-spun $Zr_{66.7-x}Ni_{33.3}M_x$ (M = Si, Pd and La and x = 0, 1, 3 at.%) alloys quenched at 3000 rpm.

which can improve the packing density and stabilize the amorphous alloy against crystallization. The strong interaction of Zr–Pd (ΔH_{mix}, $-91\,kJ\,mol^{-1}$[15]) may also enhance the thermal stability of the amorphous alloy during heating. Therefore, to a certain extent, selecting additional elements with appropriate atomic sizes can effectively improve GFA and/or enhance thermal stability of amorphous alloys.

4. Conclusions

In summary, there exists the correlation among atomic sizes of additional elements, GFA and thermal stability of Zr–Ni-based amorphous alloys with different elemental additions. Minor additions of La, Pd and Si can improve GFA of Zr–Ni-based alloys and La exhibits the optimum effect on improving GFA. The efficient cluster packing model shows that elemental additions with appropriate atomic sizes can be effective to enhance GFA of amorphous alloys.

The activation energy for crystallization of the Zr–Ni-based amorphous alloys with Si, Pd and La additions is obviously higher than that of the $Zr_{66.7}Ni_{33.3}$ amorphous alloys, and increases with decreasing distance between neighboring atoms. The thermal stability has a relation with topological short-range ordering of amorphous alloys. Moreover, the addition of small atoms is beneficial to thermal stability of amorphous alloys due to stronger short-range ordering. The effect of Pd addition on the thermal stability is also superior to La addition. So the small or intermediate atom addition can produce better effect on thermal stability of amorphous alloys than the large atom addition.

Acknowledgements

The authors acknowledge financial support from the National Natural Science Foundation of China (No. 50801031), Science and Technology Foundation of University of Jinan (No. xky0802) and Doctoral Foundation of University of Jinan. The authors also thank support from the Key Subject (Laboratory) Research Foundation of Shandong Province.

References

[1] J. Saida, T. Sanada, S. Sato, M. Imafuku, E. Matsubara, A. Inoue, J. Alloys Compd. 434–435 (2007) 135.
[2] H.J. Chang, E.S. Park, Y.S. Jung, M.K. Kim, D.H. Kim, J. Alloys Compd. 434–435 (2007) 156.
[3] J.B. Qiang, W. Zhang, A. Inoue, Mater. Sci. Eng. B 148 (2008) 114.
[4] V.D. Louzguine-Luzgin, L.V. Louzguina-Luzgina, G.Q. Xie, S. Li, W. Zhang, A. Inoue, J. Alloys Compd. 460 (2008) 409.
[5] C.M. Zhang, X. Hui, Z.G. Li, G.L. Chen, J. Alloys Compd. 467 (2009) 241.
[6] J.K. Lee, W.T. Kim, D.H. Kim, Mater. Lett. 57 (2003) 1514.
[7] W.H. Wang, Z. Bian, P. Wen, Y. Zhang, M.X. Pan, D.Q. Zhao, Intermetallics 10 (2002) 1249.
[8] B. Zhang, D.Q. Zhao, M.X. Pan, R.J. Wang, W.H. Wang, Acta Mater. 54 (2006) 3025.
[9] X.K. Xi, L.L. Li, B. Zhang, W.H. Wang, Y. Wu, Phys. Rev. Lett. 99 (2007) 095501.
[10] W.H. Wang, Prog. Mater. Sci. 52 (2007) 540.
[11] Y. Wang, H.R. Geng, Z.X. Yang, X.Y. Teng, G.R. Zhou, J. Non-Cryst. Solids 354 (2008) 3984.
[12] Y. Wang, H.R. Geng, Y.Z. Wang, J. Non-Cryst. Solids 355 (2009) 464.
[13] Z.P. Lu, C.T. Liu, J. Mater. Sci. 39 (2004) 3965.
[14] O.N. Senkov, D.B. Miracle, Mater. Res. Bull. 36 (2001) 2183.
[15] F.R. Boer, R. Boom, W.C.M. Matterns, A.R. Miedema, A.K. Niessen, Cohesion in Metals, North-Holland, Amsterdam, 1989.
[16] R. Li, S.J. Pang, C.L. Ma, T. Zhang, Acta Mater. 55 (2007) 3719.
[17] X.M. Huang, C.T. Chang, Z.Y. Chang, X.D. Wang, Q.P. Cao, B.L. Shen, A. Inoue, J.Z. Jiang, J. Alloys Compd. 460 (2008) 708.
[18] E.S. Park, J.S. Kyeong, D.H. Kim, Scripta Mater. 57 (2007) 49.
[19] T. Abe, M. Shimono, K. Hashimoto, K. Hono, H. Onodera, Scripta Mater. 55 (2006) 421.
[20] D.B. Miracle, Acta Mater. 54 (2006) 4317.
[21] H.E. Kissinger, Anal. Chem. 29 (1957) 1702.
[22] H.R. Wang, Y.L. Gao, G.H. Min, X.D. Hui, Y.F. Ye, Phys. Lett. A 314 (2003) 81.
[23] S.V. Madge, A.L. Greer, Mater. Sci. Eng. A 375–377 (2004) 759.
[24] S. Sharma, C. Suryanarayana, Scripta Mater. 58 (2008) 508.
[25] A. Inoue, T. Zhang, T. Masumoto, J. Non-Cryst. Solids 156–158 (1993) 473.
[26] A. Inoue, Acta Mater. 48 (2000) 279.
[27] A. Inoue, T. Zhang, M.W. Chen, T. Sakurai, J. Mater. Res. 15 (2000) 2195.
[28] K.W. Park, J. Jang, M. Wakeda, Y. Shibutanic, J.C. Lee, Scripta Mater. 57 (2007) 805.